An Integrated Deterministic and Probabilistic Safety Assessment of Multi-Unit Small Modular Reactors considering the degradation of shared safety features

Stefano Marchetti[a], Francesco Di Maio[a], Enrico Zio[b,a]

[a]Energy Department, Politecnico di Milano, Milano 20156, Italy
[b]MINES Paris-PSL, Centre de Recherche sur les Risques et les Crises (CRC), Sophia Antipolis, France.

Abstract

Multi-Unit (MU) Nuclear Power Plants (NPPs) share safety features. As these may degrade in time, we propose a framework of Integrated Deterministic and Probabilistic Safety Assessment (IDPSA) to consider their time-dependent fragility. Physics-of-Failure (PoF) models of the shared safety features fragility are embedded into a dynamic model of the accident scenario evolution, whose uncertainties are accounted for by Monte Carlo simulation. We apply the proposed framework to a case study concerning a MUNPP composed of four Small Modular Dual Fluid Reactors (SMDFRs) sharing the Emergency Core Cooling Systems (ECCSs) and the Emergency Diesel Generators (EDGs). The results show the effectiveness of the framework in providing a dynamic risk picture that accounts for the degradation of shared safety features.

Keywords: Small Modular Reactors (SMRs), Multi-Unit Nuclear Power Plant (MUNPP), Shared safety features, Safety features degradation, Integrated Deterministic and Probabilistic Safety Assessment (IDPSA), Dynamic physical model.

Acronyms

AFS	Auxiliary Feedwater System
AGAN	As Good As New
AGAO	As Good As Old
CCF	Common Cause Failure
CCMT	Cell-to-Cell Mapping Technique
CDF	Core Damage Frequency
CP	Coolant Pipe
DET	Dynamic Event Tree
DHR	Decay Heat Removal
ECCS	Emergency Core Cooling System
EDG	Emergency Diesel Generator
ET	Event Tree
FT	Fault Tree
HD	High Dependency
IDPSA	Integrated Deterministic and Probabilistic Safety Assessment
IE	Initiating Event
LD	Low Dependency
LOCA	Loss Of Coolant Accident
LOP	Loss Of Power
LWR	Light Water Reactor
MD	Medium Dependency
MSR	Molten Salt Reactor
MU	Multi-Unit
MUPSA	Multi-Unit Probabilistic Safety Assessment
NPP	Nuclear Power Plant
NRC	Nuclear Regulatory Commission
PGA	Peak Ground Acceleration
PoF	Physics-of-Failure
PPU	Pyrochemical Processing Unit
SMDFR	Small Modular Dual Fluid Reactor
SMR	Small Modular Reactor
ZD	Zero Dependency

Symbols

N	Number of units
j	Index of ECCS
w	Index of EDG
i	Index of units
s	Index of safety features
N_s	Number of safety features

ΔN_s	Number of shared safety features
τ	System age
$P_{f,s}$	Failure probability of the *s-th* safety feature
$P_{f,s}^{I}$	Failure probability due to internal causes of the *s-th* safety feature
$P_{f,s}^{E}$	Failure probability due to external causes of the *s-th* safety feature
H	Hazard magnitude
P_i	Failure probability of the *i-th* unit
P_z^S	Probability of *z-th* scenario
m	Index of Monte Carlo trial
M	Number of Monte Carlo trials
$\dot{m}_{leak}$	Leak mass flow rate
t_r	Response time
Δt_m	Time between two successive maintenance interventions
S	Strength
L	Load
d	Pipe wall thickness
d_c	Corrosion defect depth
d_{in}^c	Initial depth of corrosion defect
d_r^c	Corrosion rate
$\phi[\cdot]$	Cumulative distribution function of the standard normal distribution
R	Structural seismic response
C	Seismic capacity
R_m	Median structural seismic response
C_m	Median seismic capacity
β_R	Logarithmic standard deviation of R
β_C	Logarithmic standard deviation of C
Q	Confidence level
$P_{f,EDG}^1$	Probability of failure of one EDG
$P_{f,EDG}^2$	Probability of failure of two EDGs due to CCF
α	Alpha-factor model parameter
n_{ECCS}	Number of ECCS involved in CCF event
T_w	Cladding temperature
$T_{w,nom}$	Nominal peak cladding temperature
$T_{w,fail}$	Threshold cladding temperature
T_s	Simulation time
σ_{th}	Thermal stress
E	Young modulus
γ	Coefficient of thermal expansion
σ_{UTS}	Ultimate tensile strength
f_{PGA}	Earthquake magnitude-frequency curve

$P_{LOCA,i}$	Probability of LOCA in the *i-th* unit
P_{LOP}	Probability of LOP
$A_{m,LOP}$	Median ground acceleration capacity of power infrastructure
F_i	Number of simulations that lead to the failure of the *i-th* unit
F_z^S	Number of simulations that lead to the occurrence of the *z-th* failure scenario
τ_E	Effective age of a maintained component
β	Maintenance effectiveness
$\dot{m}_c$	Coolant mass flow rate
ρ	Density
v	Velocity
A	Cross-sectional area

1. Introduction

Multi-Unit (MU) Nuclear Power Plants (NPPs) share some safety features (e.g., Emergency Core Cooling System (ECCS), Decay Heat Removal (DHR)…) ([1], [2], [3], [4]). These features may degrade in time ([5], [6], [7], [8], [9]) and this must be accounted for in the risk assessment.

To do this, in this work we propose a framework to integrate the age-dependent fragility of the shared safety features into an Integrated Deterministic and Probabilistic Safety Assessment (IDPSA). IDPSA combines deterministic and probabilistic approaches of safety assessment to overcome the limitations of static logic models [10] (such as Fault Trees (FTs) [11] and Event Trees (ETs) [12]). Typically, dynamic simulators of the system behaviour are coupled with probabilistic models to account for uncertainties (e.g., hazard magnitude, component failure times…). A number of methodologies have been developed for IDPSA (e.g., Cell-to-Cell Mapping Technique (CCMT) ([13], [14]), Dynamic Event Tree (DET) ([15], [16]), GO-FLOW methodology [17], Adaptive simulation ([18], [19]), Monte Carlo Dynamic Event Tree (MCDET) [20], Genetic Algorithm-based Dynamic Probabilistic Risk Assessment (GA-DPRA) [21], Analysis of Dynamic Accident Progression Trees (ADAPT) [22] etc.). In this work, age-dependent fragility surfaces based on tailored Physics-of-Failure (PoF) fragility models [23] are embedded in a dynamic model capable of accounting for equipment sharing, coupled with a Monte Carlo simulation scheme to account for the involved uncertainties (e.g., the magnitude of the hazard, the failure time and response time of the safety features,…).

The proposed framework is applied to a MUNPP composed by $N = 4$ units of Small Modular Dual Fluid Reactors (SMDFRs) exposed to the hazard of earthquakes. SMDFR is an innovative fast reactor design whose high operating temperatures make it ideal for hydrogen production [24]. For safety reasons, the NPP is equipped with $j = 1, \dots, 4$ shared ECCSs that provide auxiliary coolant mass flow rate to the SMDFR coolant circuit in case of Loss Of Coolant Accident (LOCA), and with $w = 1,2$ shared Emergency Diesel Generators (EDGs) to be used in case of Loss Of Power (LOP). Fragility surfaces are defined for the safety features to calculate their age-dependent failure probability. These

are used as inputs to a dynamic physical model that simulates the accident scenario. Integration within a Monte Carlo simulation scheme allows estimating the failure probability of the units of the MUNPP. The comparison of the results with the estimated values of Core Damage Frequency (CDF) of MUNPPs made of either Gen-III Light Water Reactors (LWRs) or other SMRs (in line with [25] and [1], respectively) confirms that neglecting the sharing of safety features may lead to overlooking accident scenarios and to underestimating the probability of multiple units failure. Also, considering perfect and imperfect safety features maintenance shows that neglecting degradation can lead to overly optimistic risk estimates.

The remainder of the paper is organized as follows: Section 2 illustrates the proposed framework of simulation and analysis; Section 3 presents the case study; Section 4 shows the results of the application of the proposed framework to the case study; in Section 5, conclusions are drawn.

2. A framework of IDPSA for MUPSA with aging safety features

Let us consider a MUNPP, composed of $i = 1,2, \dots, N$ units, and equipped with $s = 1,2, \dots, N_s$ safety features, among which ΔN_s are shared among the N units. The MUNPP is exposed to natural hazards, e.g. earthquakes. To account for aging of the shared safety features the following steps are carried out (**Fig. 1**):

1) Characterize:
    a. the natural hazard, by the magnitude-frequency curve;
    b. the system response to the hazard, in particular in terms of:
        b.i. the safety features performance, by age-dependent fragility surfaces;
        b.ii. the Common Cause Failures (CCFs) of the ΔN_s shared safety features, by CCF models;
2) Define a dynamic model of the accident scenario evolution;

3) Calculate the system failure probability at each age τ, by integrating the dynamic model into a Monte Carlo simulation scheme to account for the uncertainties therein.

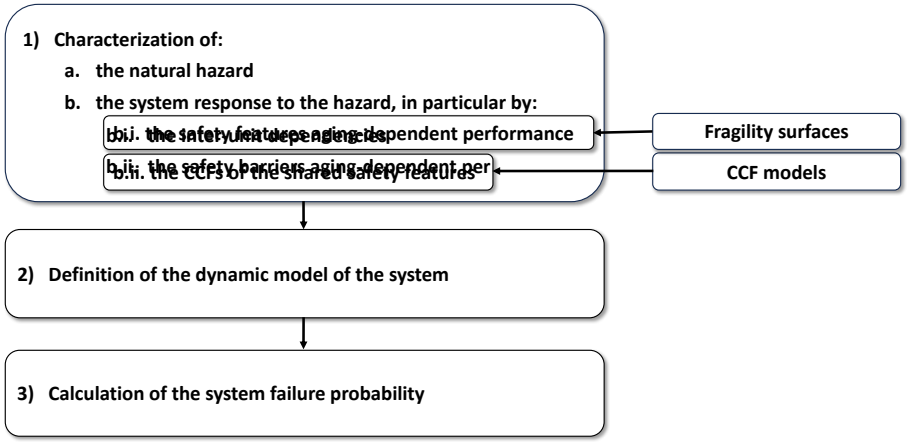

Fig.1. Flowchart of the proposed framework.

2.1 Hazard and system characterization

Natural hazards are typically characterized by a magnitude-frequency curve, extracted from historical data. The system response to a hazard depends on its physical properties, layout, subsystems and components, also possibly shared among different units of the system.

Each $s = 1,2,\dots,N_s$ safety feature in the system is characterized by a response time $t_{r,s}$ and a failure probability $P_{f,s}$ (see Eq. 1); the latter is composed of the probability of failure due to internal causes ($P_{f,s}^{I}$) and due to external hazards ($P_{f,s}^{E}$), both functions of the age τ and the latter also of the hazard magnitude H [23]:

$$P_{f,s}(H,\tau) = P_{f,s}^{I}(\tau) + P_{f,s}^{E}(H,\tau) - P_{f,s}^{I}(\tau)\cdot P_{f,s}^{E}(H,\tau) \quad [1]$$

In particular, $P_{f,s}^{I}(\tau)$ can be computed by a degradation model (e.g., a pipe corrosion degradation model with a threshold-based failure criterion on the pipe thickness [26]), whereas $P_{f,s}^{E}(H,\tau)$ can be calculated using a fragility surface obtained integrating PoF-based aging models into the fragility model of the specific safety feature exposed to the specific natural hazard [23].

The probability of CCF among the shared safety features is assessed by typical CCF models, such as:

- alpha-factor model [27]; for a subgroup of $N_A \in \Delta N_s$ shared safety features, CCF factors $\alpha_1, \alpha_2, \dots, \alpha_{N_A}$ are defined and the probabilities of failure of groups of $1,2, \dots, N_A$ safety features (i.e., $P_{f,s}^1, P_{f,s}^2, \dots, P_{f,s}^{N_A}$) are calculated:

$$\begin{aligned} P_{f,s}^1 &= \alpha_1 P_{f,s} \\ P_{f,s}^2 &= \alpha_2 P_{f,s} \\ &\dots \\ P_{f,s}^{N_A} &= \alpha_{N_A} P_{f,s} \end{aligned} \quad [2]$$

- dependency evaluation tree [28]; for a subgroup of $N_B \in \Delta N_s$ shared safety features, a dependency evaluation tree (e.g., **Fig. 2,** where ZD stands for "Zero Dependency", LD stands for "Low Dependency", MD stands for "Medium Dependency" and HD stands for "High Dependency") is used to evaluate the dependency among the features.

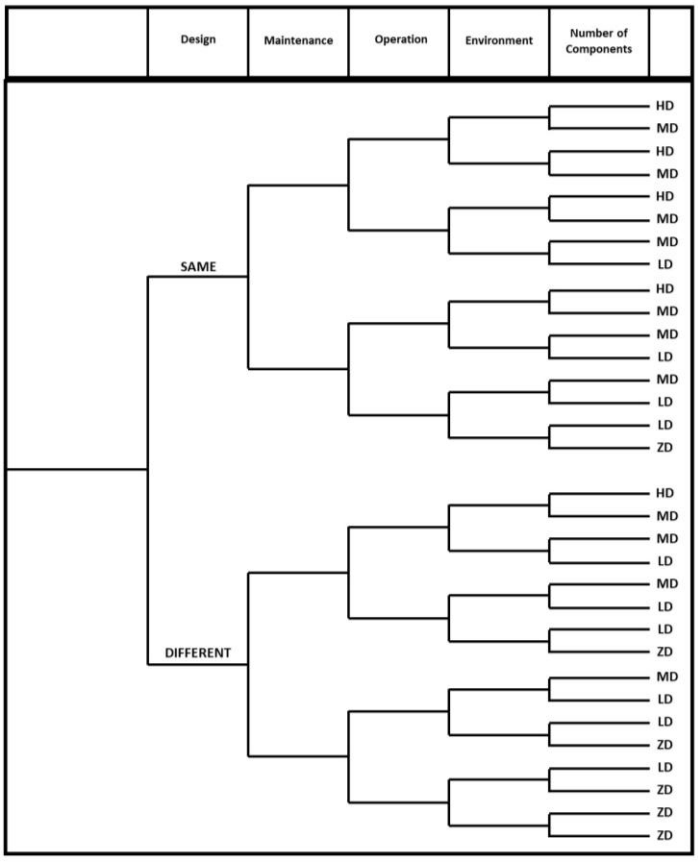

Fig. 2. Dependency evaluation tree [28].

Then, the probability associated with each CCF combination is calculated as follows [28]:

$$P_{s,CCF}(n_B) = \sum_{b=1}^{n_B} \left(P_{f,b} \cdot \prod_{c=1, c \neq b}^{n_B} P_{CCF,c}(b) \right) \quad [3]$$

where n_B is the number of safety features involved in the CCF combination and $P_{CCF,c}(b)$ is the probability of failure of the *c-th* safety feature conditioned to the failure of the *b-th* safety feature, defined as in **Tab. 1**.

Tab. 1. Conditional failure probabilities.

Dependency level	Conditional probability
ZD	$P_{CCF,c} = P_{f,c}$
LD	$P_{CCF,c} = \frac{1 + 19P_{f,c}}{20}$
MD	$P_{CCF,c} = \frac{1 + 6P_{f,c}}{7}$
HD	$P_{CCF,c} = \frac{1 + P_{f,c}}{2}$

2.2 Dynamic model of accident evolution

The parameters values defined in Section 2.1 (i.e., $t_{r,s}, P_{f,s}$ and the CCF probabilities) are fed to a dynamic model to simulate the evolution of the accident scenarios in terms of relevant safety parameters.

2.3 System failure probability calculation

Simulations are performed to quantify the failure probability at each age τ of single units and groups of units (P_i with $i = 1,2, \dots, N$ and P_z^S with $z = 1,2, \dots, N$, respectively), conditioned to the accidental scenario occurred. To account for uncertainties (e.g., in the hazard magnitude, safety features failure times and response times,…) Monte Carlo simulation of M alternative scenario conditions is performed. A flowchart of the procedure for the simulation is provided in **Fig. 3**.

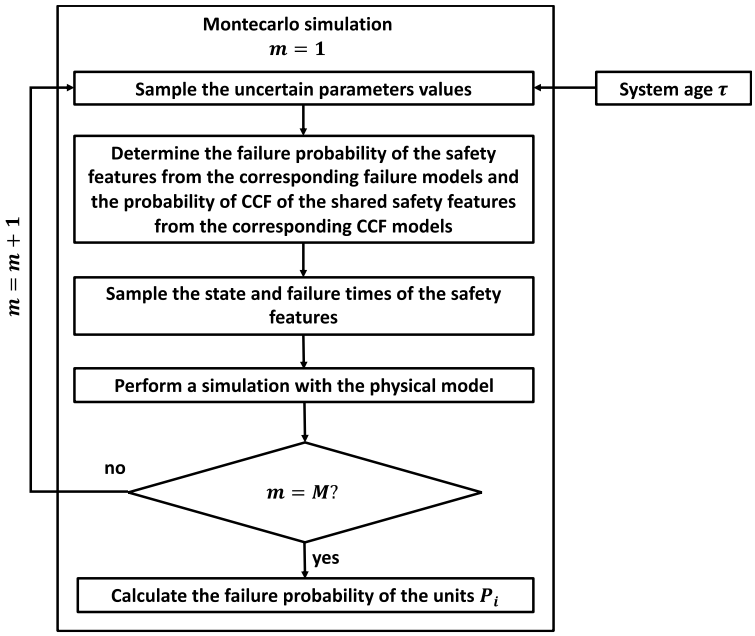

Fig.3. Flowchart of the Monte Carlo simulation scheme.

3. Case study

The case study regards a MUNPP composed of $N = 4$ SMDFRs units [24]. In **Fig. 4**, one SMDFR is shown. In this novel reactor design, the liquid fuel, which is a mixture of uranium tetrachloride and plutonium tetrachloride, enters the core vessel at the bottom, spreads over a system of vertical tubes that provide enough surface for the heat transfer and leaves the reactor from the top, towards the Pyrochemical Processing Unit (PPU). The liquid coolant, which is pure lead, enters the core vessel from the bottom, removes the heat from the fuel tubes by conduction and leaves the vessel from the top towards the heat exchanger. The design life of the system is assumed to be equal to 60 years [29].

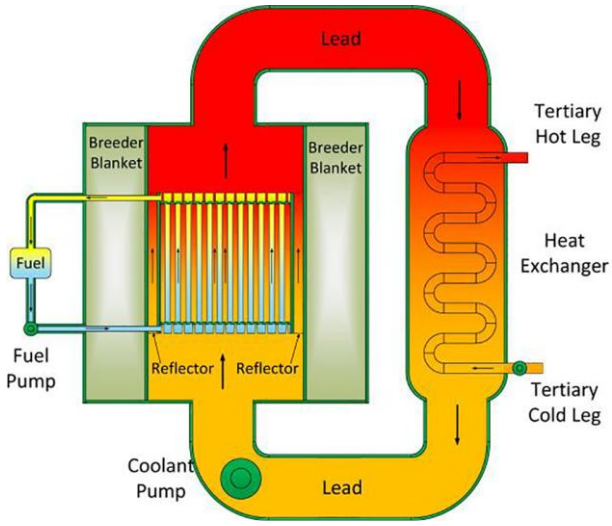

Fig.4. Sketch of the SMDFR [30].

The design parameters of the SMDFRs units (all identical) are reported in **Tab. 2**.

Tab. 2. Design properties of the SMDFR [31].

Parameter	Value
Core zone $D\ x\ H$ [m]	$0.95\ x\ 2.0$
Distribution zone $D\ x\ H$ [m]	$0.95\ x\ 0.2$
Collection zone $D\ x\ H$ [m]	$0.95\ x\ 0.2$
Height of the core [m]	2.4
Outer reflector diameter [m]	1.25
Tank $D\ x\ H$ [m]	$1.65\ x\ 3.4$
Number of fuel tubes	1027
Fuel pin pitch [m]	0.025
Outer/interior fuel tube diameter [m]	0.008/0.007
Outer/interior coolant tube diameter [m]	0.005/0.004
Mean linear power density [W/cm]	609
Thermal power [MW]	250
Fuel inlet temperature [K]	1300
Coolant inlet temperature [K]	973
Nominal peak cladding temperature [K], $T_{w,nom}$	1150
Fuel inlet velocity [m/s]	3
Coolant inlet velocity [m/s]	5

3.1 Hazard and system characterization

The considered Initiating Event (IE) is the occurrence of an earthquake with Peak Ground Acceleration (PGA) $PGA \in [0, 19.62] \frac{m}{s^2}$. The magnitude-frequency curve is taken from [32] and shown in **Fig. 5**. It is important to note that:

- the magnitude-frequency curve does not correspond to a site-specific design basis earthquake, nor it is intended to relate to the natural frequencies of the safety-related systems;
- all safety features are assumed to be located at the same elevation and exposed to a seismic wave with a single, fixed direction.

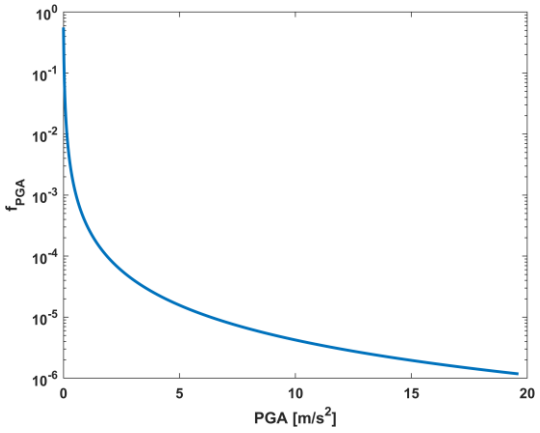

Fig. 5. Earthquake magnitude-frequency curve.

For illustrative purposes and without loss of generality, it is assumed that the earthquake occurrence leads only to a LOCA with the leak flow rate $\dot{m}_{leak}$ shown in **Fig. 6**, which mimics the flow rate of conventional LWRs during LOCA [33].

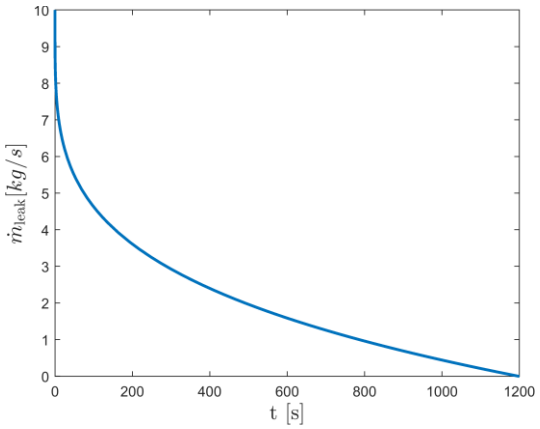

Fig. 6. LOCA leak flow rate.

To prevent the occurrence of a LOCA, the NPP is equipped with stainless steel Coolant Pipes (CPs); to mitigate the consequences of a LOCA, the NPP is equipped with $j = 1, \dots, 4$ ECCSs (one for each unit, with a modular piping system that allows for the sharing of flow among all units, while guaranteeing that each ECCS can perform its safety function independently from the others, in line with the design criteria of the Nuclear Regulatory Commission (NRC) [34] and $w = 1,2$ EDGs (shared among all units, with each EDG being capable of providing power to all ECCSs in case of LOP [35]) (**Tab.3**).

Tab. 3. Safety features employed in the system.

Safety Feature	**Classification**	**Description**
Coolant Pipes (CP)	Passive, Preventive	Liquid lead containment
Emergency Core Cooling System (ECCS)	Active, Mitigative	Auxiliary coolant delivery in case of LOCA
Emergency Diesel Generator (EDG)	Active, Mitigative	Independent source of power in case of LOP

The considered safety features are actuated on demand with an uncertain response time $t_{r,s}$ (**Tab. 4**, second column) and maintained each $\Delta t_{m,s}$ (**Tab. 4**, third column). The value of $\Delta t_{m,ECCS}$ is assumed equal to that of an Auxiliary Feedwater System (AFS) of a typical light water reactor [36]; furthermore, $\Delta t_{m,CP}$ is necessarily synchronous to the periodic drainage of coolant and fuel from the reactor.

Tab. 4. Safety features employed in the system.

Safety Feature	$\boldsymbol{t_{r,s}}$	$\boldsymbol{\Delta t_{m,s}}$
Coolant Pipe (CP)	$t_{r,CP} = 0$	$3\ y$
Emergency Core Cooling System (ECCS)	$t_{r,ECCS} \sim [30,60]\ s$ [37]	$0.5\ y$ [36]

Emergency Diesel Generator (EDG)	$t_{r,EDG}$~[60,300] s [38]	1.5 y [39]

The failure probabilities $P_{f,s}$, $P_{f,s}^{I}$ and $P_{f,s}^{E}$ are assessed as follows:

1. CP:

   a. $P_{f,CP}^{I}$ is assessed with a load strength model [40]:

$$P_{f,CP}^{I}(\tau) = P(S_{CP} \leq L_{CP}(\tau)) \quad [4]$$

   where L_{CP} is the load, i.e., the depth of the water pitting corrosion on the pipes $d_{CP}^{c}(\tau)$, whose initial value $d_{in,CP}^{c}$ is assumed to follow a normal distribution $d_{in,CP}^{c} \sim N(1.59\ mm, 0.619\ mm)$ [41], and S_{CP} is the strength, i.e., 80% of the thickness of the pipe. CP is considered failed if the pipe thickness is equal or lower than 20% of its initial value. The increase in d_{CP} is calculated using a corrosion rate $d_{r,CP}^{c} = 1.1 \frac{mm}{year}$ [26]. The resulting $P_{f,CP}^{I}$ is shown in **Fig. 7** as a function of age.

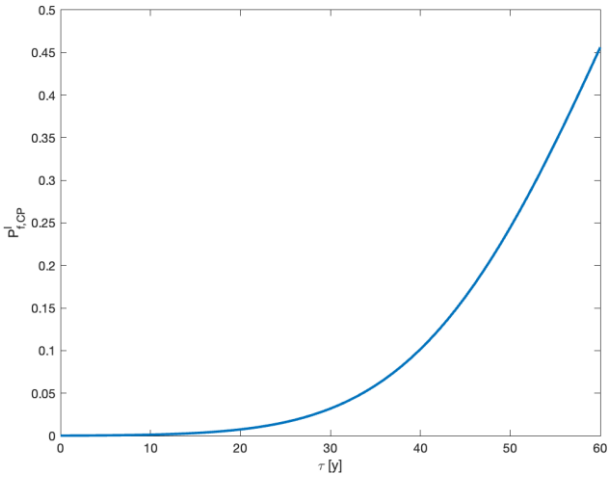

Fig. 7. $P_{f,CP}^{i}$ as a function of age.

   b. $P_{f,CP}^{E}$ is assessed with a fragility surface obtained integrating the fragility model from [42] with the data from [43], which relates the seismic capacity to the thickness of the pipe, leading to the fragility surface of Eq. (5):

$$P_{f,CP}^{E}(PGA, \tau) = \phi\left[\frac{ln\left(R_{m,CP}(PGA)\right) - ln\left(C_{m,CP}(\tau)\right)}{\sqrt{\beta_{C_{CP}}^{2} + \beta_{R_{CP}}^{2}}}\right] \quad [5]$$

where $\phi[\cdot]$ is the cumulative distribution function of the standard normal distribution, $R_{m,CP}$ and $C_{m,CP}$ are the CP median structural seismic response and the age-dependent median seismic capacity, respectively, and $\beta_{R_{CP}} = 0.07$ and $\beta_{C_{CP}} = 0.14$ are the logarithmic standard deviations of R_{CP} and C_{CP}. The resulting fragility surface is shown in **Fig. 8**.

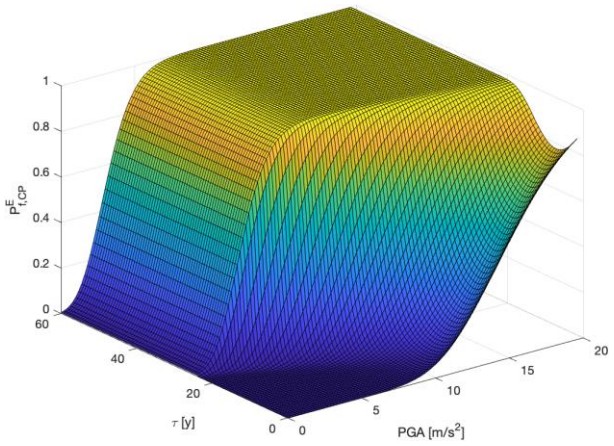

Fig. 8. $P^E_{f,CP}$ as a function of age and PGA.

2. ECCS:

   a. $P^I_{f,ECCS}$ is assessed with a load strength model:

$$P^I_{f,ECCS}(\tau) = P(S_{ECCS} \leq L_{ECCS}(\tau)) \quad [6]$$

where L_{ECCS} is the load, i.e., the depth of the water pitting corrosion on the pipes $d^c_{ECCS}(\tau)$, whose initial value $d^c_{in,ECCS}$ is assumed to follow the same normal distribution as $d^c_{in,CP}$, and S_{ECCS} is the strength, i.e., 80% of the thickness of the pipe. The increase in d^c_{ECCS} is calculated using a corrosion rate $d^c_{r,ECCS} < d^c_{r,CP}$, since the liquid lead is not flowing inside the ECCS pipes. The decrease in corrosion rate due to the absence of flow is estimated following [44], leading to $d^c_{r,ECCS} = 0.55\,\frac{mm}{year}$ [44]. $P^I_{f,ECCS}$ is shown in **Fig. 9** as a function of age.

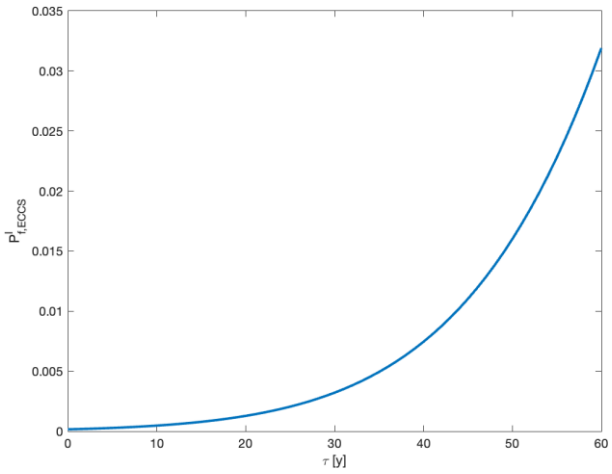

Fig. 9. $P^i_{f,ECCS}$ as a function of age.

b. $P^E_{f,ECCS}$ is computed with Eq. (5), using the data in [43] together with $d^c_{r,ECCS}$ to calculate the decrease in seismic capacity of ECCS pipes, leading to the fragility surface shown in **Fig. 10**.

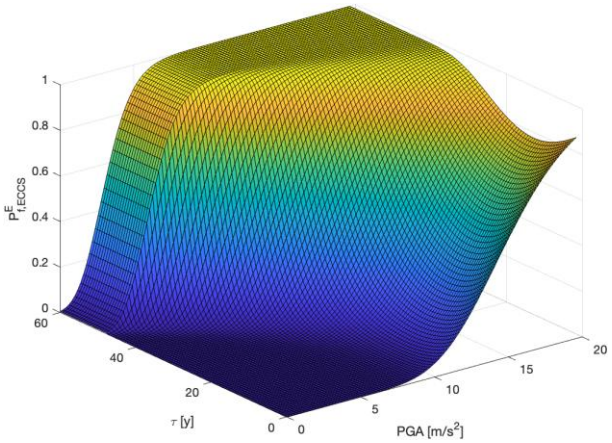

Fig. 10. $P^E_{f,ECCS}$ as a function of age and PGA.

3. EDG:

a. the failure of EDG due to internal causes is assumed to be induced by its cooling pipes failure [45]. $P^I_{f,EDG}$ is computed with a load-strength model:

$$P^I_{f,EDG}(\tau) = P(S_{EDG} \leq L_{EDG}(\tau)) \quad [7]$$

where L_{EDG} is the load, i.e., the depth of the water pitting corrosion on the cooling pipes $d^c_{EDG}(\tau)$, whose initial value $d^c_{in,EDG}$ is assumed to follow the same normal

distribution as $d^c_{in,CP}$, and S_{EDG} is the strength, i.e., 80% of the thickness of the pipe. The increase of $d^c_{EDG}(\tau)$ is calculated using the corrosion rates of **Tab. 5**. $P^I_{f,EDG}$ is shown in **Fig. 11** as a function of age.

Tab. 5. EDG corrosion rates [46].

Exposure time t_e $[days]$	$d^c_{r,EDG}$ $[mm/y]$
$t_e \leq 497$	0.52
$497 < t_e \leq 759$	0.52
$759 < t_e \leq 780$	0.42
$780 < t_e \leq 1116$	0.43
$t_e \geq 1116$	0.42

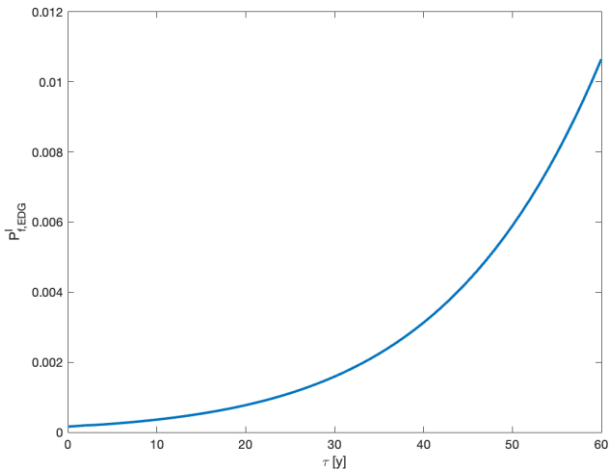

Fig. 11. $P^I_{f,EDG}$ as a function of age.

b. $P^E_{f,EDG}$ is computed with a fragility surface obtained integrating the fragility model from [47] with the seismic capacity degradation data from [43], leading to the fragility surface of Eq. (8):

$$P^E_{f,EDG}(PGA,\tau) = \phi\left[\frac{ln\left(\frac{PGA}{C_{m,EDG}}\right) + \beta_U \phi^{-1}(Q)}{\beta_R}\right] \quad [8]$$

where $C_{m,EDG}$ is the median seismic capacity of EDG, $Q = 0.95$ is the confidence level, $\beta_U = 0.26$ and $\beta_R = 0.24$. The resulting fragility surface is shown in **Fig. 12**.

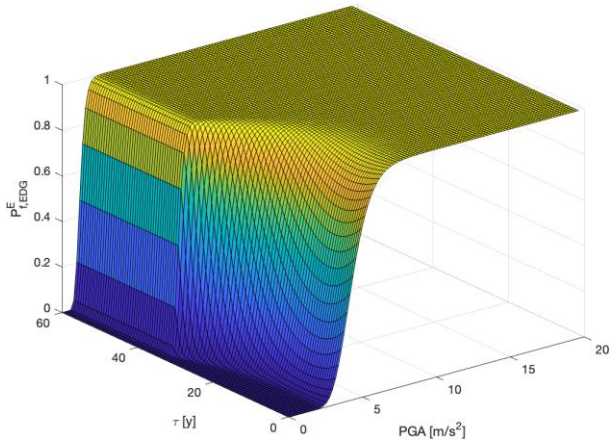

Fig. 12. $P^e_{f,EDG}$ as a function of age and PGA.

Notice that a seismic event leading to the failure of CP, and therefore to a LOCA, would also likely cause the failure of the EDG, since $P^E_{f,EDG} \geq P^E_{f,CP}$ across all PGA values and system ages τ.

The inter-unit failure dependencies are accounted for by considering the possible CCFs among EDGs and ECCSs as follows:

- To model the probabilities of occurrence of CCF events involving one or two EDGs, an alpha-factor model is developed, based on historical data (**Fig. 13** shows the count of CCF events for each sub-system of EDGs [48]), an alpha-factor model is used [27]:

$$P^1_{f,EDG} = \alpha_1 P_{f,EDG} \quad [9]$$
$$P^2_{f,EDG} = \alpha_2 P_{f,EDG} \quad [10]$$

where $P^1_{f,EDG}$ and $P^2_{f,EDG}$ are the probabilities that only one EDG fails and that both fail due to CCF, respectively, $\alpha_1 = 0.9881$ and $\alpha_2 = 0.0119$ [49].

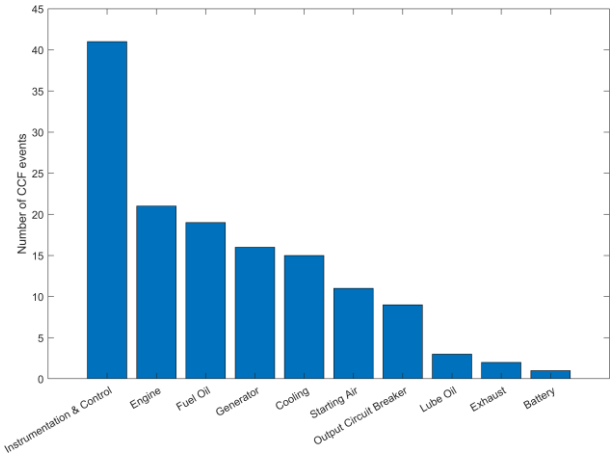

Fig. 13. CCF events involving each EDG sub-system.

- Historical data on ECCS are, instead, not available because of the SMDFR being a new design; the dependency evaluation tree of **Fig. 2** [28] is, thus, used to evaluate the dependency among the different ECCSs. We assume that the ECCSs are HD among each other, since in the considered MUNPP they share the same design, maintenance team, operation mode, environment and a number of components. Therefore, the probability of the CCF combinations is calculated as [28]:

$$P_{ECCS,CCF}(n_{ECCS}) = n_{ECCS} \cdot P_{f,ECCS} \cdot \left(\frac{1 + P_{f,ECCS}}{2}\right)^{n_{ECCS}-1} \quad [11]$$

where n_{ECCS} is the number of ECCSs involved in the CCF group.

3.2 Monte Carlo-based integrated dynamic probabilistic model

The dynamic model developed [31] (see the brief description provided in Appendix A) simulates safe and accidental conditions transients that might occur in the system. The Monte Carlo simulation takes as input the actual age of the system $\tau \in [0,60]$ y and proceeds as shown in **Fig. 14** to provide in output the peak cladding temperature $T_{w,i}(t)$ of each *i-th* reactor of the MUNPP over a time horizon $T_s = 1200$ s, which is the time allowed to confirm that the drainage of the fuel from the reactor core through the melting fuel plug is successful ([24], [50], [51]), and thus the accident is successfully mitigated.

The threshold cladding temperature not to be exceeded during the accident is $T_{w,fail} = 1244\ K$, as results from the solution of Eq. (12) of the thermal stress on the fuel pipes:

$$\sigma_{th} = E\gamma(T)\Delta T \quad [12]$$

where $E = 207\ GPa$ is the Young's Modulus of Nickel 201, which is the candidate material for Molten Salt Reactors (MSRs) [52], $\gamma(T)$ is the temperature-dependent coefficient of thermal expansion (estimated interpolating the data in [53]) and ΔT is the resulting temperature change of the fuel pipes to the ultimate tensile strength of the pipe, $\sigma_{max} = \sigma_{UTS} = 345\ MPa$ ($\Delta T_{fail} = 94\ °C$ and $T_{w,fail} = T_{w,nom} + \Delta T_{fail} = 1244\ K$).

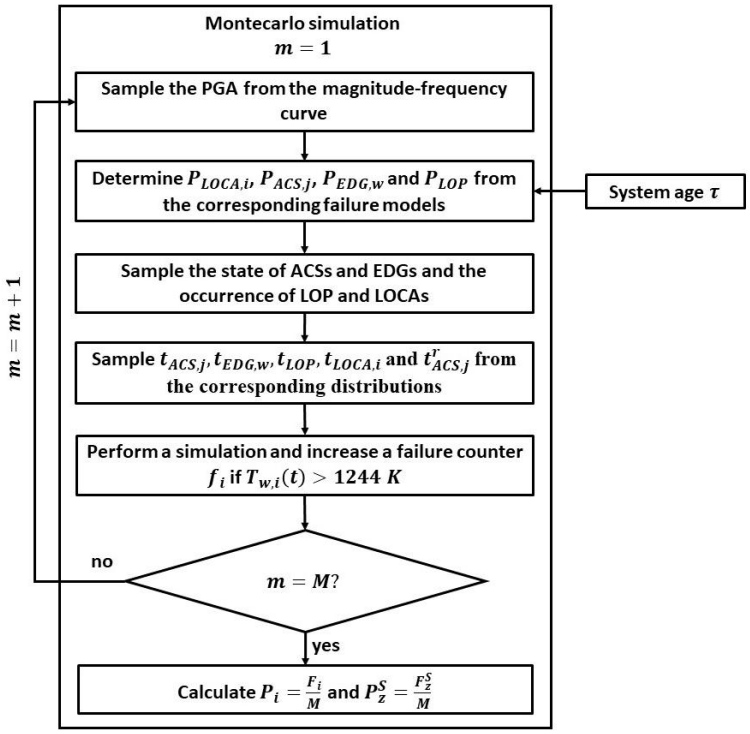

Fig.14. Monte Carlo simulation flowchart.

A Monte Carlo simulation of M trials is performed to calculate the failure probability P_i of each reactor and of group of reactors P_z^S (where $S = 1,2,3,4$ corresponds to the failure of one, two, three and four reactors, respectively), as follows:

1. the earthquake PGA is sampled from the magnitude-frequency curve (f_{PGA}) of the site;
2. τ and PGA are used to determine:

2.1. the probability of LOCA occurrence of each reactor $P_{LOCA,i} = P_{f,CP,i}$, as described in Section 3.1;

2.2. the failure probability of each ECCS $P_{f,ECCS,j}$, as described in Section 3.1;

2.3. the failure probability of each EDG $P_{f,EDG,w}$, as described in Section 3.1;

2.4. the probability of LOP P_{LOP}, assessed with the following fragility model [54]:

$$P_{LOP}(PGA) = \phi\left[\frac{ln\left(\frac{PGA}{A_{m,LOP}}\right) + \beta_{U,LOP}\phi^{-1}(Q)}{\beta_{R,LOP}}\right] \quad [13]$$

where $A_{m,LOP} = 0.2\ g$ is the time-dependent median ground acceleration capacity, Q is the confidence level, $\beta_{U,LOP} = 0.25$ and $\beta_{R,LOP} = 0.2$;

3. the probabilities determined in Step 2 and the CCF models of Section 3.1 are used to sample the state of ECCSs and EDGs, and the occurrence of LOP and LOCA;

4. the failure events occurrence times (i.e., $t_{ECCS,j}, t_{EDG,w}, t_{LOP}$ and $t_{LOCA,i}$) and the response times of each ECCS and each EDG (i.e., $t^r_{ECCS,j}$, $t^r_{EDG,w}$) are sampled from the corresponding distributions (**Tab. 6**);

5. the simulation of the dynamic model is performed and, for each *i-th* unit, the output values $T_{w,i}$ are obtained to determine whether the unit is failed or not. In **Fig. 15,** two examples of $T_{w,1}$ transients are shown: on the left, after the initial rise in temperature due to a LOCA at $t = 365\ s$, the activation of the ECCS around $t = 800\ s$ causes the temperature to decrease and, then, stabilize; on the right, the unmitigated rise in temperature due to a LOCA at $t = 50\ s$ leads to the reactor failure around $t = 700\ s$;

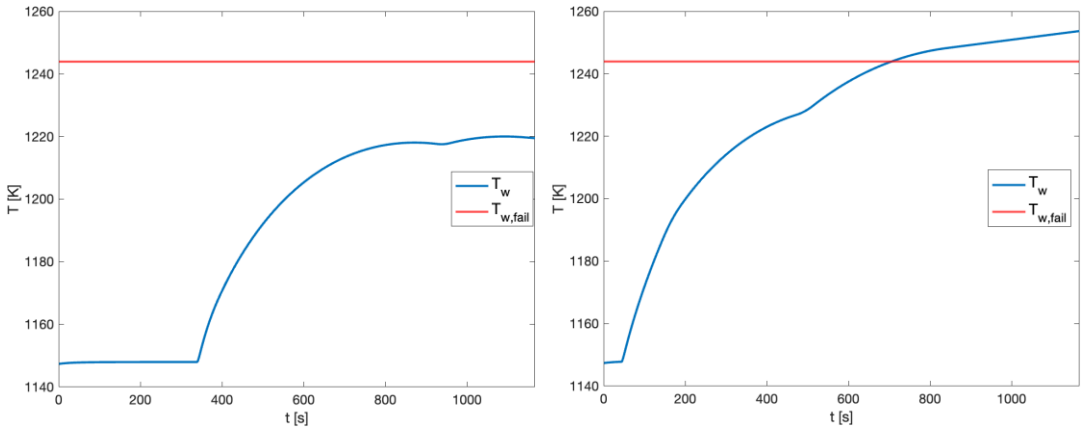

Fig. 15. Example transients of $T_{w,1}$. On the left a safe transient and on the right a failed transient. The solid straight line indicates the failure threshold.

6. M trials are repeated from Step 1;
7. finally, P_i and P_z^S are calculated as follows:

$$P_i = \frac{F_i}{M} \quad [14]$$

$$P_z^S = \frac{F_z^S}{M} \quad [15]$$

where F_i is the number of simulations that lead to the failure of the *i-th* unit and F_z^S is the number of simulations that lead to the occurrence of the *z-th* scenario.

Tab. 6. Distributions of the uncertain failure and response times.

Variable	Description	Distribution
t_{EDG}	Failure time of EDG [s]	$t_{EDG} \sim U(0,500)\ s$
t_{ECCS}	Failure time of ECCS [s]	$t_{ECCS} \sim U(0,500)\ s$
t_{LOP}	Time of LOP [s]	$t_{LOP} \sim logN(3.30,1)\ s$
t_{LOCA}	Time of LOCA [s]	$t_{LOCA} \sim logN(3.30,1)\ s$
t_{ECCS}^r	Response time of ECCS [s]	$t_{ECCS}^r \sim U(30,90)\ s$[37]
$t_{EDG,w}^r$	Response time of EDG [s]	$t_{EDG}^r \sim U(10,180)\ s$[55]

4. Results

The framework presented in Section 2 has been applied to the case study of Section 3. In **Fig. 16** and **Fig. 17**, we show the estimates of P_i and P_z^S, $z = 1,2,3,4$, respectively, at the end of the design life (i.e., at $\tau = 60\ y$) for the MUSMDFR, in comparison with the typical values of CDF of Gen-III LWRs (see [25], [56]) and of a MUNPP comprised of other SMRs (see [1]), when neither the degradation of safety features nor the contribution to the CDF of the sharing of safety features are considered.

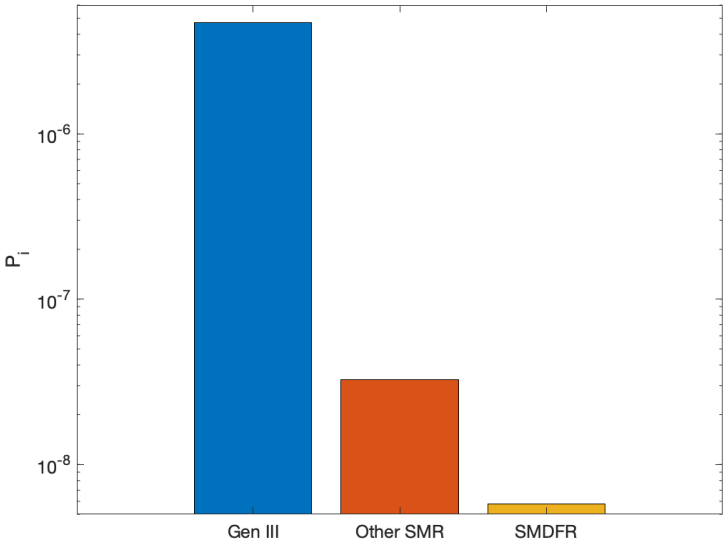

Fig. 16. Comparison of P_i, neglecting safety features degradation.

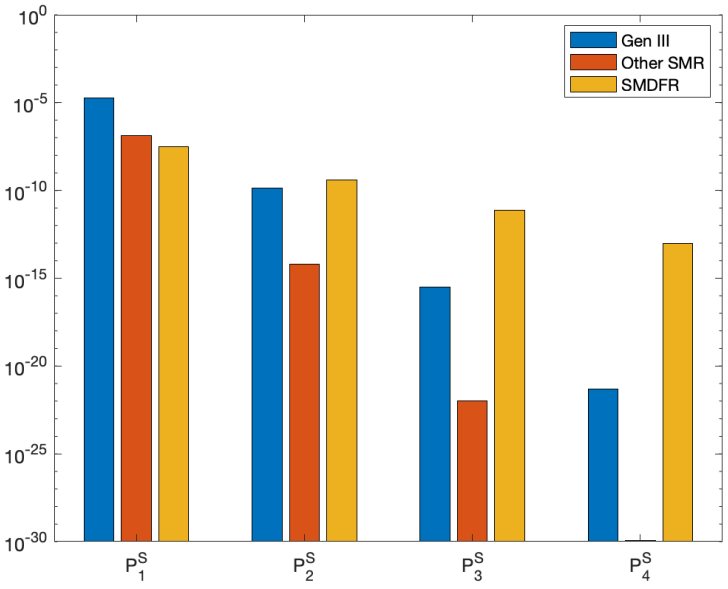

Fig. 17. Comparison of P_z^S, neglecting safety features degradation.

As shown in **Fig. 16**, both MUSMRs and MUSMDFRs achieve failure probability values lower than the current threshold of acceptability (i.e., $P_{i,threshold} = 10^{-5}$ [57]), meaning that SMDFRs can be regarded as safe as other SMR designs (limited to LOCAs triggered by seismic events). On the other hand, **Fig. 17** highlights the importance of considering the sharing of safety features when conducting a MUPSA: whereas MUSMDFRs and MUSMRs have similar probabilities of single unit failure (i.e., P_1^S), the probabilities of multiple reactor failures (i.e., P_2^S, P_3^S and P_4^S) in MUSMDFRs are several orders of magnitude larger than those in MUSMRs; such difference is due to neglecting the effect of sharing safety features in the risk assessment of MUSMRs.

To show the impact of the safety features degradation on the MUSMDFRs risk assessment, in **Fig. 18** and **Fig. 19** we compare the values of P_i and P_z^S obtained neglecting safety features degradation with the ones obtained considering degradation with models described in Section 3.1 and the maintenance schedule of **Tab. 4**, under two different assumptions:

1. Perfect maintenance (i.e., the safety features are restored As Good As New (AGAN) upon maintenance);
2. Imperfect maintenance (i.e., the degradation of the safety features is reduced but not eliminated by the maintenance intervention [58]). To do this, we use the imperfect maintenance model described in ([59], [60]), which allows calculating the effective age of the maintained component as follows:

$$\tau_E^k = \tau_E^{k-1} + \beta \Delta t_m \quad [16]$$

where τ_E^k is the effective age immediately after the *k-th* maintenance intervention, $\beta \in [0,1]$ is the effectiveness of the maintenance intervention ($\beta = 0$ represents perfect maintenance, i.e. AGAN; $\beta = 1$ represents completely ineffective maintenance, i.e. As Good As Old (AGAO)) and Δt_m is the time between two successive maintenance interventions. Without loss of generality, we assume $\beta = 0.1$.

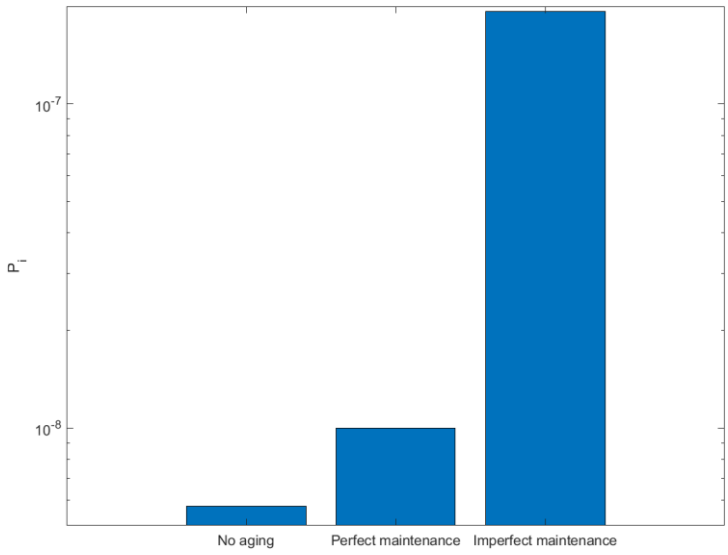

Fig. 18. Results for P_i considering perfect and imperfect maintenance.

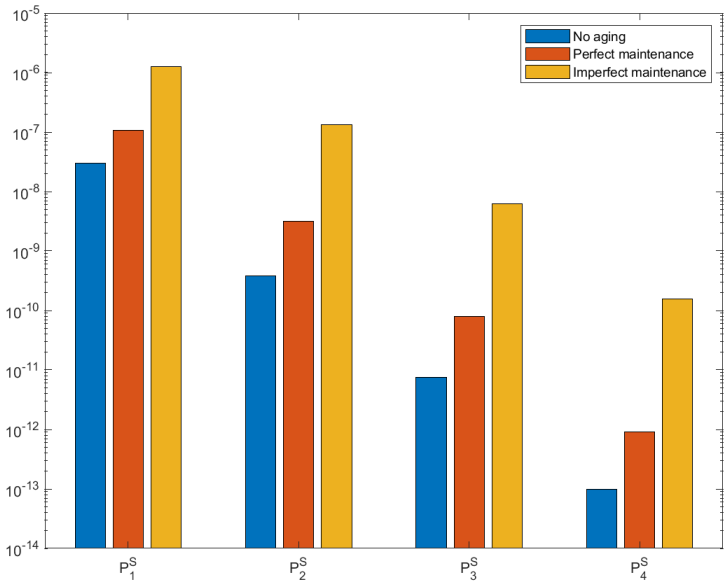

Fig. 19. Results for P_z^S considering perfect and imperfect maintenance.

As expected, **Fig.18** and **Fig. 19** show that the degradation of the aging safety features leads to an increase in the failure probability of the reactors, especially in the case of imperfect maintenance. The causes of such increase are twofold: firstly, the employment of a highly corrosive coolant, and secondly the suboptimal maintenance strategy outlined in **Tab. 4**, which is based on typical maintenance schedules of existing nuclear reactors (for ECCS and EDG) and on expert-judgement (for CP). To further illustrate the impact of degradation under imperfect maintenance, **Fig. 20** shows the values of P_i at different system ages: a P_i increase is observed at 60 years of operation,

emphasizing the importance of reviewing the system conditions, as customary, after the first 40 years of operation, prior to any decision regarding the extension of the system life to 60 years or beyond

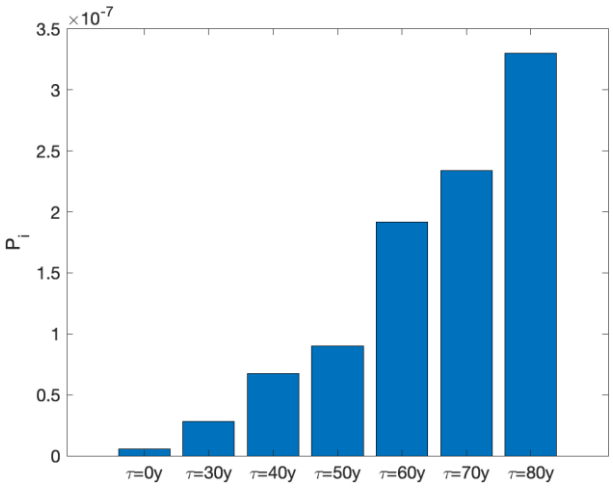

Fig. 20. Values of P_i at different system ages considering imperfect maintenance.

The results presented highlight that neglecting the degradation of safety features leads to an underestimation of the risk and possibly to suboptimal decision making, especially in case of reactors employing highly corrosive coolants, such as the SMDFR.

5. Conclusions

A novel IDPSA framework has been proposed for the risk assessment of MUNPPs, accounting for shared safety features and their degradation. The inter-unit failure dependencies among the shared safety features have been modelled by classical CCF models and the degradation of the safety features has been accounted for by integrating PoF-based aging models into the features fragility models, so as to define tailored fragility surfaces. A dynamic model has been developed to simulate accidental scenarios, within a Monte Carlo simulation scheme to account for uncertainties.

The proposed framework has been applied to a case study regarding a MUNPP composed of four units of SMDFR exposed to earthquake hazard. The results show the relevance of considering both the sharing and the degradation of safety features for the risk value of MUNPPs: neglecting these could lead to overly optimistic risk estimates.

Appendix A: The MUSMDFR simulation model

The developed model simulates four units of SMDFR, each consisting of a core described by two models: a neutronic model and a thermal-hydraulic model, linked by the reactivity feedback.

To capture the neutronic behaviour of the SMDFR, a modified point kinetic model with 6 delayed neutron groups is adopted to account for the flowing of the fuel: even if the fuel outside the core is kept subcritical, the decay process of delayed neutron precursors has to be considered to evaluate its impact on the neutron distribution in the core. This is done considering two additional terms: the precursor loss when the fuel leaves the core, and the precursor gain when the fuel re-enters the core [31]. Then, a thermal-hydraulic model is built based on the assumption that the fuel, piping wall and coolant in the core are divided into 3 parts and each part has lumped propertied [31].

To model the occurrence of a LOCA, the following assumptions are made:

- the LOCA flow rate $\dot{m}_{leak}$ mimics the one that might occur in conventional reactors [33], leading to:

$$\dot{m}_{leak} = \dot{m}_{leak,0} + a \cdot t^b \quad [17]$$

  where $\dot{m}_{leak,0} = 18 \frac{kg}{s}$ is the initial value of the leak flow rate and a and b are parameters. We assume that, without loss of generality, $a = 3$ and $b = \frac{1}{4}$.

- the velocity imposed by the pump on the coolant is constant. Therefore, the flow rate of the coolant $\dot{m}_c$ decreases as the total coolant mass decreases due to air entering the pipes. This change is due to the reduced density of the fluid in the pipe cross-section, since the mass flow rate of a pump $\dot{m}$ can be expressed as:

$$\dot{m} = \rho v A \quad [18]$$

  where ρ is the density of the fluid, v is the constant velocity of the fluid and A is the cross-sectional area. Therefore, we can calculate $\dot{m}_c$ as follows:

$$\dot{m}_c = \dot{m}_{c,0} \cdot \frac{\rho_{lead} \cdot a + \rho_{air} \cdot (1 - a)}{\rho_{lead}} \quad [19]$$

where $\dot{m}_{c,0}$ is the nominal coolant mass flow rate, ρ_{lead} is the density of liquid lead, ρ_{air} is the density of air and a is the fraction of the total coolant mass that has been leaked.

Finally, to mitigate the accidental scenario that follows the LOCA, the mitigative action of ECCS is modelled as a constant flow rate of liquid lead, leading to:

$$\dot{m}_{c,tot} = \dot{m}_c + \dot{m}_{c,ACS} \quad [20]$$

Acknowledgement

This study was developed within the research project "ARtificial Intelligence and STOchasTic simulation for the rEsiLience of critical infrastructurES - ARISTOTELES" funded by MIUR – Italian Ministry for Scientific Research under the PRIN 2022 program (grant 2022TAFXZ5) and by the European Union – Next Generation EU program.

References

[1] F. Di Maio, L. Bani, and E. Zio, 'Seismic resilience assessment of Small Modular Reactors by a Three-loop Monte Carlo Simulation', *Nuclear Engineering and Design*, vol. 410, p. 112385, Aug. 2023, doi: 10.1016/J.NUCENGDES.2023.112385.

[2] J. Lamarsh, 'SAFETY CONSIDERATIONS IN THE DESIGN AND OPERATION OF LIGHT WATER NUCLEAR POWER PLANTS', *Ann N Y Acad Sci*, vol. 365, 1981.

[3] J. Xing, Z. Zeng, and E. Zio, 'Joint optimization of safety barriers for enhancing business continuity of nuclear power plants against steam generator tube ruptures accidents', *Reliab Eng Syst Saf*, vol. 202, p. 107067, Oct. 2020, doi: 10.1016/J.RESS.2020.107067.

[4] V. Hassija, C. Senthil Kumar, and K. Velusamy, 'Probabilistic safety assessment of multi-unit nuclear power plant sites - An integrated approach', *J Loss Prev Process Ind*, vol. 32, no. 1, pp. 52–62, 2014, doi: 10.1016/j.jlp.2014.07.013.

[5] S. Marchetti, F. Di Maio, E. Zio, L. Decarli, L. La Rosa, and G. Nicotra, 'Key performance indicators for aging safety barriers in oil and gas facilities', in *European Conference On Safety And Reliability (ESREL)*, 2023, pp. 2230–2235. doi: 10.3850/978-981-18-8071-1_P708-cd.

[6] F. Di Maio, S. Marchetti, and E. Zio, 'Robust multi-objective optimization of safety barriers performance parameters for NaTech scenarios risk assessment and management', *Reliab Eng Syst Saf*, p. 109245, Jul. 2023, doi: 10.1016/j.ress.2023.109245.

[7] F. Di Maio, S. Marchetti, and E. Zio, 'A framework of sensitivity analysis for the performance assessment of safety barriers impacted by NaTech accidents', *Process Safety and Environmental Protection*, vol. 171, pp. 1022–1030, Mar. 2023, doi: 10.1016/j.psep.2022.08.072.

[8] S. D. Unwin, P. P. Lowry, and M. Y. Toyooka, 'Reliability models of aging passive components informed by materials degradation metrics to support long-term reactor operations', *Nuclear Science and Engineering*, vol. 171, no. 1, 2012, doi: 10.13182/NSE11-18.

[9] S. E. Aumeier, B. Alpay, J. C. Lee, and A. Z. Akcasu, 'Probabilistic techniques for diagnosis of multiple component degradations', *Nuclear Science and Engineering*, vol. 153, no. 2, 2006, doi: 10.13182/NSE06-A2599.

[10] E. Zio, 'Integrated deterministic and probabilistic safety assessment: Concepts, challenges, research directions', *Nuclear Engineering and Design*, vol. 280, pp. 413–419, 2014, doi: 10.1016/j.nucengdes.2014.09.004.

[11] R. Flage, P. Baraldi, E. Zio, and T. Aven, 'Probability and Possibility-Based Representations of Uncertainty in Fault Tree Analysis', *Risk Analysis*, vol. 33, no. 1, pp. 121–133, 2013, doi: 10.1111/j.1539-6924.2012.01873.x.

[12] D. Huang, T. Chen, and M. J. J. Wang, 'A fuzzy set approach for event tree analysis', *Fuzzy Sets Syst*, vol. 118, no. 1, pp. 153–165, Feb. 2001, doi: 10.1016/S0165-0114(98)00288-7.

[13] B. Tombuyses and T. Aldemir, 'CONTINUOUS CELL-TO-CELL MAPPING', *J Sound Vib*, vol. 202, no. 3, pp. 395–415, May 1997, doi: 10.1006/JSVI.1996.0835.

[14] P. Wang and T. Aldemir, 'Some improvements in state/parameter estimation using the cell-to-cell mapping technique', *Nuclear Science and Engineering*, vol. 147, no. 1, 2004, doi: 10.13182/NSE04-A2415.

[15] F. Di Maio, C. Picoco, and E. Zio, 'A repairable dynamic event tree framework for the safety assessment of a steam generator of a nuclear power plant', in *PSAM 2016 - 13th International Conference on Probabilistic Safety Assessment and Management*, 2017.

[16] B. Cohn, T. Noel, J. Cardoni, T. Haskin, D. Osborn, and T. Aldemir, 'Integrated Safety and Security Analysis of Nuclear Power Plants Using Dynamic Event Trees', *Nuclear Science and Engineering*, vol. 197, no. sup1, 2023, doi: 10.1080/00295639.2023.2177076.

[17] T. Matsuoka and M. Kobayashi, 'GO-FLOW: A New Reliability Analysis Methodology', *Nuclear Science and Engineering*, vol. 98, no. 1, pp. 64–78, 1988, doi: 10.13182/NSE88-A23526.

[18] P. Turati, N. Pedroni, and E. Zio, 'An Adaptive Simulation Framework for the Exploration of Extreme and Unexpected Events in Dynamic Engineered Systems', *Risk Analysis*, vol. 37, no. 1, pp. 147–159, Jan. 2017, doi: 10.1111/risa.12593.

[19] P. Turati, N. Pedroni, and E. Zio, 'Simulation-based exploration of high-dimensional system models for identifying unexpected events', *Reliab Eng Syst Saf*, vol. 165, pp. 317–330, Sep. 2017, doi: 10.1016/J.RESS.2017.04.004.

[20] M. Kloos and J. Peschke, 'MCDET: A probabilistic dynamics method combining Monte Carlo simulation with the discrete dynamic event tree approach', *Nuclear Science and Engineering*, vol. 153, no. 2, 2006, doi: 10.13182/NSE06-A2601.

[21] Y. Vorobyev and P. Kudinov, 'Development and application of a genetic algorithm based dynamic pra methodology to plant vulnerability search', in *International Topical Meeting on Probabilistic Safety Assessment and Analysis 2011, PSA 2011*, 2011.

[22] A. Hakobyan *et al.*, 'Dynamic generation of accident progression event trees', *Nuclear Engineering and Design*, vol. 238, no. 12, 2008, doi: 10.1016/j.nucengdes.2008.08.005.

[23] S. Marchetti, F. Di Maio, and E. Zio, 'A Physics-of-Failure (PoF) model-based Dynamic Bayesian Network for considering the aging of safety barriers in the risk assessment of industrial facilities', *J Loss Prev Process Ind*, vol. 91, p. 105402, Oct. 2024, doi: 10.1016/J.JLP.2024.105402.

[24] A. Huke, G. Ruprecht, D. Weißbach, S. Gottlieb, A. Hussein, and K. Czerski, 'The Dual Fluid Reactor - A novel concept for a fast nuclear reactor of high efficiency', *Ann Nucl Energy*, vol. 80, pp. 225–235, 2015, doi: 10.1016/j.anucene.2015.02.016.

[25] M. Prasad, G. Vinod, A. J. Gaikwad, and A. Ramarao, 'Site core damage frequency for multi-unit Nuclear Power Plants site', *Progress in Nuclear Energy*, vol. 96, pp. 56–61, Apr. 2017, doi: 10.1016/J.PNUCENE.2016.12.007.

[26] J. Zhang, 'A review of steel corrosion by liquid lead and lead–bismuth', *Corros Sci*, vol. 51, no. 6, pp. 1207–1227, Jun. 2009, doi: 10.1016/J.CORSCI.2009.03.013.

[27] A. Mosleh, 'A multi-parameter, event-based common-cause failure model', *SMiRT9 Paper No. M7/3*, 1987.

[28] S. Jang and M. Jae, 'A development of methodology for assessing the inter-unit common cause failure in multi-unit PSA model', *Reliab Eng Syst Saf*, vol. 203, p. 107012, Nov. 2020, doi: 10.1016/J.RESS.2020.107012.

[29] B. Una *et al.*, 'Simulation of the NuScale SMR and Investigation of the Effect of Load-Following on Component Lifetimes', *Nucl Technol*, vol. 210, no. 1, pp. 1–22, 2024, doi: 10.1080/00295450.2023.2216973.

[30] M. Wang, X. He, R. Macian-Juan, and X. Wang, 'One-dimensional transient analysis of the dual-fluid reactor system', *Ann Nucl Energy*, vol. 162, Nov. 2021, doi: 10.1016/j.anucene.2021.108481.

[31] C. Liu, R. Luo, and R. Macián-Juan, 'A new uncertainty-based control scheme of the small modular dual fluid reactor and its optimization', *Energies (Basel)*, vol. 14, no. 20, Oct. 2021, doi: 10.3390/en14206708.

[32] H. Shahraki and N. Shabakhty, ‘Seismic Performance Reliability of RC Structures: Application of Response Surface Method and Systemic Approach’, *Civil Engineering Infrastructures Journal*, vol. 48, no. 1, pp. 47–68, 2015.

[33] J. H. Park, Y. J. An, K. H. Yoo, and M. G. Na, ‘Leak flow prediction during loss of coolant accidents using deep fuzzy neural networks’, *Nuclear Engineering and Technology*, vol. 53, no. 8, pp. 2547–2555, Aug. 2021, doi: 10.1016/j.net.2021.01.040.

[34] Nuclear Regulatory Commission (NRC), ‘Westinghouse AP1000 Design Control Document ’, 2011.

[35] J. R. Willis, ‘Modeling of emergency diesel generators in an 800 megawatt nuclear power plant’, *IEEE Transactions on Energy Conversion*, vol. 8, no. 3, 1993, doi: 10.1109/60.257056.

[36] A. Volkanovski and L. Cizelj, ‘Nuclear Power Plant Maintenance Optimization with Heuristic Algorithm’, *Science and Technology of Nuclear Installations*, vol. 2014, p. 458016, 2014, doi: 10.1155/2014/458016.

[37] United States Nuclear Regulatory Commission, ‘Auxiliary Feedwater System’, 2002. Accessed: Mar. 19, 2024. [Online]. Available: https://www.nrc.gov/docs/ML0307/ML030760397.pdf

[38] H. G. Lim, J. E. Yang, and M. J. Hwang, ‘A quantitative analysis of a risk impact due to a starting time extension of the emergency diesel generator in optimized power reactor-1000’, *Reliab Eng Syst Saf*, vol. 92, no. 7, pp. 961–970, Jul. 2007, doi: 10.1016/J.RESS.2006.07.004.

[39] United States Nuclear Regulatory Commission, ‘Emergency Diesel Generators’, 2011. Accessed: Mar. 19, 2024. [Online]. Available: https://www.nrc.gov/docs/ML1122/ML11229A061.html

[40] K. Yang, ‘Failure probability evaluation for normally distributed load-strength model with unknown parameters’, *Reliab Eng Syst Saf*, vol. 51, no. 1, pp. 115–118, Jan. 1996, doi: 10.1016/0951-8320(95)00103-4.

[41] W. Zhou, ‘Reliability Evaluation of Corroding Pipelines Considering Multiple Failure Modes and Time-Dependent Internal Pressure’, *Journal of Infrastructure Systems*, 2011, doi: 10.1061/(ASCE).

[42] B. G. Jeon, S. W. Kim, D. W. Yun, D. Hahm, and S. Eem, ‘Seismic Fragility Evaluation of Main Steam Piping of Isolated APR1400 NPP Considering the Actual Failure Mode’, *Sustainability (Switzerland)*, vol. 14, no. 14, Jul. 2022, doi: 10.3390/su14148315.

[43] U.S. Nuclear Regulatory Commission, ‘Risk-Informed Assessment of Degraded Buried Piping Systems in Nuclear Power Plants’, 2005. Accessed: Mar. 21, 2024. [Online]. Available: https://www.nrc.gov/docs/ML0516/ML051650146.pdf

[44] F. Balbaud-Célérier and F. Barbier, ‘Investigation of models to predict the corrosion of steels in flowing liquid lead alloys’, *Journal of Nuclear Materials*, vol. 289, no. 3, pp. 227–242, Mar. 2001, doi: 10.1016/S0022-3115(01)00431-7.

[45] M. Zhegang, ‘INL/RPT-22-66601, Enhanced Component Performance Study: Emergency Diesel Generators 1998–2020’, 2022.

[46] O. J. Van Der Schijff and S. C. Bodemann, ‘Corrosion of Piping in Dry and Preaction Fire Sprinkler Systems: Interim Results of Long Term Corrosion Testing Under Compressed Air and Nitrogen Supervision’, in *Corrosion 2013*, [Online]. Available: http://southteksystems.com/

[47] Y. Wang, L. Li, and D. Wang, ‘A study of seismic probability safety assessment for a typical three-loop pressurized water reactor nuclear power plant’, in *25th International Conference on Nuclear Engineering*, 2017.

[48] Idaho National Engineering and Environmental Laboratory, 'NUREG/CR-68 19, Vol. 1, Common-Cause Failure Event Insights - Emergency Diesel Generators', 1999.

[49] D. Il Kang, M. J. Hwang, S. H. Han, and J. E. Yang, 'Approximate formulas for treating asymmetrical common cause failure events', *Nuclear Engineering and Design*, vol. 239, no. 2, pp. 346–352, Feb. 2009, doi: 10.1016/J.NUCENGDES.2008.10.004.

[50] X. Wang, 'Draining Time of the Dual Fluid Reactor', in *12th International Topical Meeting on Nuclear Reactor Thermal-Hydraulics, Operation and Safety (NUTHOS-12)*, 2018. [Online]. Available: https://www.researchgate.net/publication/325846731

[51] M. Ilham and T. Okawa, 'A Simple Analytical Model to Predict the Freeze Plug Opening Time in Molten Salt Reactors', *Journal of Nuclear Engineering and Radiation Science*, vol. 9, no. 4, Jul. 2023, doi: 10.1115/1.4062879.

[52] G. A. Young and T.-L. Sham, 'Initial assessment of metallurgical interaction of clad/base metal systems', Argonne, IL (United States), Sep. 2018. doi: 10.2172/1506992.

[53] Special Metals, 'Datasheet of Nickel 201 thermo mechanical properties'. Accessed: May 21, 2024. [Online]. Available: https://www.specialmetals.com/documents/technical-bulletins/nickel-200.pdf

[54] J. Ryu and M. Jae, 'A quantification methodology of Seismic Probabilistic Safety Assessment for nuclear power plant', *Ann Nucl Energy*, vol. 159, Sep. 2021, doi: 10.1016/j.anucene.2021.108296.

[55] H. G. Lim, J. E. Yang, and M. J. Hwang, 'A quantitative analysis of a risk impact due to a starting time extension of the emergency diesel generator in optimized power reactor-1000', *Reliab Eng Syst Saf*, vol. 92, no. 7, pp. 961–970, Jul. 2007, doi: 10.1016/j.ress.2006.07.004.

[56] K. Ebisawa, T. Teragaki, S. Nomura, H. Abe, M. Shigemori, and M. Shimomoto, 'Concept and methodology for evaluating core damage frequency considering failure correlation at multi units and sites and its application', *Nuclear Engineering and Design*, vol. 288, pp. 82–97, Jul. 2015, doi: 10.1016/J.NUCENGDES.2015.01.002.

[57] M. Kumar, A. S. Whittaker, R. P. Kennedy, J. J. Johnson, and A. Kammerer, 'Seismic probabilistic risk assessment for seismically isolated safety-related nuclear facilities', *Nuclear Engineering and Design*, vol. 313, 2017, doi: 10.1016/j.nucengdes.2016.12.031.

[58] M. Zanotelli, J. W. Hines, and J. B. Coble, 'Combining Similarity Measures and Left-Right Hidden Markov Models for Prognostics of Items Subjected to Perfect and Imperfect Maintenance', *Nuclear Science and Engineering*, 2024, doi: 10.1080/00295639.2024.2303165.

[59] M. Kijima, 'Some Results for Repairable Systems with General Repair', *J Appl Probab*, vol. 26, no. 1, pp. 89–102, 1989, doi: 10.2307/3214319.

[60] M. Kijima, H. Morimura, and Y. Suzuki, 'Periodical replacement problem without assuming minimal repair', *Eur J Oper Res*, vol. 37, no. 2, pp. 194–203, Nov. 1988, doi: 10.1016/0377-2217(88)90329-3.